

Excited states of lutetium oxide and its singly charged cation

Accepted Manuscript: This article has been accepted for publication and undergone full peer review but has not been through the copyediting, typesetting, pagination, and proofreading process, which may lead to differences between this version and the Version of Record.

Cite as: J. Chem. Phys. (in press) (2022); <https://doi.org/10.1063/5.0084483>

Submitted: 06 January 2022 • Accepted: 31 January 2022 • Accepted Manuscript Online: 31 January 2022

Lu Wu,  George Schoendorff, Yuchen Zhang, et al.



View Online



Export Citation



CrossMark

The Journal
of Chemical Physics

SPECIAL TOPIC: Low-Dimensional
Materials for Quantum Information Science

Submit Today!



Excited states of lutetium oxide and its singly charged cation

Lu Wu,^a George Schoendorff,^{b,c} Yuchen Zhang,^a Mourad Roudjane,^a Mark S. Gordon,^{b,*} and Dong-Sheng Yang^{a,*}

^aDepartment of Chemistry, University of Kentucky, Lexington, KY 40506-0055, United States

^bDepartment of Chemistry, Iowa State University, Ames, IA 50011-3111, United States

^cPropellants Branch, Rocket Propulsion Division, Aerospace Systems Directorate, Air Force Research Laboratory, AFRL/RQRP, Edwards Air Force Base, California 93524, United States

*Authors to whom correspondence should be addressed:

dyang0@uky.edu, mark@si.msg.chem.iastate.edu.

Abstract:

Vibronic spectra of lutetium oxide (LuO) seeded in supersonic molecule beams is investigated with mass-analyzed threshold ionization (MATI) spectroscopy and second-order multiconfigurational quasi-degenerate perturbation (MCQDPT2) theory. Six states of LuO and four states of LuO⁺ are located by the MCQDPT2 calculations, and an $a^3\Pi(\text{LuO}^+) \leftarrow C^2\Sigma^+(\text{LuO})$ transition is observed by the MATI measurement. The vibronic spectra show abnormal vibrational intervals for both the neutral and cation excited states, and the abnormality is attributed to vibrational perturbations induced by interactions with neighboring states.

I. INTRODUCTION

Lutetium (Lu) is the last element in the lanthanide series of the Periodic Table and has the ground electron configuration of $4f^{14}5d6s^2$. Its electronic configuration in the 5d and 6s shells is the same as that of the first lanthanide element, lanthanum (La) ($5d6s^2$). Because the 4f shell is complete and 4f orbitals are compact, one might presume that Lu and La should have similar atomic structures and bonding characteristics with other atoms or molecules. However, the electronic structures of the two atoms are quite different as shown by the NIST atomic data base.¹ For example, the lowest excited state of La has a $5d^26s$ configuration (2668 cm^{-1}) formed by exciting a 6s electron to a 5d orbital, while the lowest excited state of Lu has a $4f^{14}6s^26p^1$ configuration (4136 cm^{-1}) formed by promoting a 6s electron to a 6p orbital. The ground configurations of both atoms are not particularly active in bonding interactions because the completely filled $6s^2$ orbital would have strong repulsion with electrons of interacting partners. The formation of the first reactive configuration of La $5d^26s$ has a relatively low-energy cost (2668 cm^{-1}), while the energy cost (18851 cm^{-1}) for the formation of the corresponding Lu $4f^{14}5d^26s$ configuration is several times higher. The different electronic structures of the two atoms suggest that their bonding will likely be different with other atoms or molecules. For metal monoxides, the reported ionization energy (IE) of LuO ($6.5\text{-}7.8\text{ eV}$)²⁻⁵ is considerably higher than that of LaO [$5.2446(6)\text{ eV}$]⁶ even though the first IEs of the two atoms are close to each other (5.5769 eV for La and 5.4259 for Lu). On the other hand, bond dissociation energies of LuO ($6.8\text{-}7.1\text{ eV}$) and LuO⁺ ($5.3\text{-}5.70\text{ eV}$) are lower than those of LaO ($8.2\text{-}8.6\text{ eV}$) and LaO⁺ ($8.7\text{-}8.9\text{ eV}$).^{3,5,7-9} It should be noted that the bond dissociation energy of LuO is higher than that of its cationic species, while the opposite is observed for LaO.

Unlike LaO, for which excited states have been extensively investigated experimentally^{7,10-15} and computationally,¹⁶⁻¹⁸ the knowledge about excited states of LuO is largely limited to early measured transitions of $A^2\Pi$, $B^2\Pi$, $C^2\Sigma^+ \leftarrow X^2\Sigma^+$ ^{7,19} and a recent *ab initio* study that used an inadequate CASSCF active space that does not include Lu 6p orbital set.²⁰ In addition to the early spectroscopic measurements on the excited states, several more recent studies have been reported on the ground states of LuO or LuO⁻.²¹⁻²³ Liu et al. reported photoelectron velocity-map imaging spectra for the $X^2\Sigma^+ (\text{LuO}) \leftarrow X^1\Sigma^+ (\text{LuO}^-)$ transition at four different photon energies and vibrational frequencies of 743(10) cm⁻¹ for the ground state of LuO⁻ and 839(10) cm⁻¹ for the ground state of LuO.²¹ Cooke et al. reported rotational spectra of LuO through cavity pulsed jet Fourier transform microwave spectroscopy and derived a series of spectroscopic constants including a harmonic frequency of 816 cm⁻¹ with anharmonicity of 2.81 cm⁻¹.²² In their studies of lanthanide atom reactions with oxygen using matrix-isolation infrared spectroscopy, Willson and Andrews reported vibrational frequencies of 829.3 and 864.9 cm⁻¹ for LuO and LuO⁺ deposited in a low-temperature Ar matrix.²³

In this article, we report an ionization transition that involves excited states of the neutral molecule and singly charged cation and the characterization of these excited states with mass-analyzed threshold ionization (MATI) spectroscopy and second-order multiconfigurational quasi-degenerate perturbation (MCQDPT2) theory. A better understanding of energy profiles of the reactive diatomic species and its cation offers the potential to improve the synthesis of stable Lu oxides and tailor their properties for specific applications.

II. EXPERIMENTAL AND COMPUTATIONAL METHODS

II A. Experimental

The metal-cluster beam instrument used in this work consists of reaction and spectroscopy vacuum chambers and was described in a previous publication.²⁴ Lu oxides were produced by laser vaporization (Lumonics YM-800 or Continuum Minilite II Nd:YAG, 532 nm) of a Lu rod (Metallium, Inc., 99.5%) in the presence of a pulse of ultra-high-purity He or Ar carrier gas delivered by a homemade piezoelectric pulsed valve.²⁵ The metal vapor and carrier gas passed down a clustering tube (2 mm inner diameter, 2 cm length), and the resultant clusters were supersonically expanded into the vacuum chamber. The supersonic jet was skimmed (2 mm diameter) 3 cm downstream from the exit of the clustering tube. A pair of deflection plates (2.5 cm spacing, 220V) located after the skimmer was used to remove residual charged species that were formed during laser ablation from the molecular beam before it entered the second chamber.

Prior to the MATI measurements, photoionization time-of-flight mass spectra were recorded to determine the chemical content of the cluster beam and pulsed-field-ionization photoionization efficiency spectra were recorded to locate the ionization threshold of LuO. With the ionization laser set above the ionization threshold, the experimental conditions (e.g., timing and power of the vaporization and ionization lasers and the backing pressure of the carrier gas) were carefully optimized to maximize the intensity of the LuO⁺ signal in the mass spectra.

With the optimized experimental conditions, LuO was excited to high-lying Rydberg states in a single-photon process by the frequency-doubled output of a dye laser (Lumonics HD-500) pumped by a Nd:YAG laser (Quanta Ray GCR-3 or Continuum Surelite, 355 nm) and ionized by an electric pulse (DEI PVM-4140, 320 V cm⁻¹). Several laser dyes including Stilbene 420, Coumarin 440, 460, 480, 500 and 540 A, or their mixtures were used to cover a spectral range as wide as possible. The laser beam was collinear and counter propagating with the molecule beam. The time delay between the laser and electric pulses was varied to maximize the MATI signal, and

it was typically 20 μs for the He carrier and 50 μs for the Ar carrier. A small DC field (3.94 V cm^{-1}) was applied to help separate the ions produced by direct photoionization from the MATI ions produced by delayed field ionization. The MATI signal was obtained by scanning the wavelength of the tunable dye laser, detected by a dual microchannel plate detector, amplified by a preamplifier (SRS SR445), averaged by a gated integrator (SRS SR250), and stored in a laboratory computer. Laser wavelengths were calibrated against titanium atomic transitions in the MATI spectral region.¹ The Stark shift induced by the DC field was calculated using the relation of $\Delta E = 6.1E_f^{1/2}$, where E_f is in V cm^{-1} and ΔE in cm^{-1} .²⁶

B. Computational

Quantum mechanical calculations were performed using the GAMESS quantum chemistry software package.²⁷ The Sapporo-DKH3-TZP-2012 basis set was used for lutetium and the Sapporo-TZP-2012 basis set was used for oxygen.^{28,29} The local unitary transformation (LUT)³⁰ of the infinite order two component (IOTC)^{31,32} method was used to account for scalar relativistic effects. Valence virtual orbitals (VVOs)³³⁻³⁵ were computed to provide a full-valence set of molecular orbitals for use in multireference calculations. The multiconfigurational self-consistent field method (MCSCF) was used to compute reference wave functions for six electronic states of the neutral molecule that were generated by permutations of the unpaired electron over the VVOs resulting in three Σ states, two Π states, and one Δ state. Likewise, the MCSCF reference wave functions were computed for the three lowest energy excited states of the cation while a restricted Hartree-Fock (RHF) reference wave function was used for the $^1\Sigma^+$ ground state of the cationic species. Dynamic correlation effects were included via the use of MCQDPT2³⁶ where the O 2s and 2p and the Lu 4f, 5s, 5p, 5d, 6s, and 6p orbitals were included in the correlation space. Orbital

plots were obtained using MacMolPlt^{37,38} and were drawn using an isosurface of 0.02 bohr^{-3/2}.

To compare with the experimental MATI spectra, Franck-Condon (FC) factors were calculated from the equilibrium geometries, harmonic vibrational frequencies, and normal coordinates of the neutral and ionized complexes from the MCQDPT2 calculations.³⁹ Spectral simulations were obtained using the experimental linewidth and Lorentzian line shape. Transitions from excited vibrational energy levels of the neutral species were considered by assuming thermal excitation at specific temperatures. Simulations were attempted at temperatures up to 1500 K, and 600 K was found to give the best matches with intensities of the hot bands of low vibrational quanta of the neutral molecules.

III. RESULTS AND DISCUSSION

Figure 1(a) presents a MATI spectrum of LuO (top, blue) seeded in a He carrier gas, which spans an energy range of $\sim 10,000$ cm⁻¹. The spectrum displays the origin band (i.e., 0-0 transition) at 44699 (5) cm⁻¹ [5.5420 (6) eV]. On the higher energy side of the origin band are four stronger vibronic bands with intervals ≥ 766 cm⁻¹, while on the lower energy side are nine weaker bands with intervals ≤ 750 cm⁻¹. The 44699 cm⁻¹ band is considered the origin band because the vibrational intervals are distinctively different on the two sides of this band. The energy intervals above the origin band ($v^+ = 1-4$) are associated with the cation, while those ($v = 1-9$) below the origin band arise from vibrational levels of the neutral molecule. The two intervals (730* cm⁻¹) labeled between $v = 3$ and $v = 5$ are the average rather than individual intervals. This is because the head of the $v = 4$ band marked with “*” is interfered by a strong Lu atomic transition 1S_0 (Lu⁺) \leftarrow $^2D_{5/2}$ (Lu), which makes it difficult to determine its exact position. There is another Lu atomic transition marked with “#” in the spectrum with the He carrier, which corresponds to 1S_0 (Lu⁺) \leftarrow

$^2D_{3/2}$ (Lu) but does not interfere with any vibronic transition of LuO. We also recorded MATI spectra with an Ar carrier, and a representative spectrum is presented in Figure 1 (b) (middle, red). The spectrum with the Ar carrier shows signals in a narrower spectral range ($\sim 6000 \text{ cm}^{-1}$). The weak bands at higher vibrational quanta of the neutral molecule ($v > 3$) are not clearly observed, suggesting the vibrational temperatures with Ar are lower than those with He. This observation is consistent with a previously observed carrier gas effect on the vibrational temperatures of metal complexes.⁴⁰⁻⁴² Another difference between the two carrier gases exists in spectral line shapes. With the molecule seeded in He, most bands have an asymmetric shape and are degraded toward the red, while the spectral bands become more symmetric with Ar. The reduction of the red-shaded asymmetric shape may be due to the reduced rotational populations with Ar. Although the rotational transitions are not resolved in the spectra, the red degradation of the vibronic band suggests an increase of the metal-oxygen bond length from the initial neutral state to the final ion state.⁴³

The MATI spectra of LuO are unlikely to be associated with the ionization of the ground-state molecule, as early measurements of reaction equilibria, mass spectrometry, and electron impact ionization efficiency indicated that the IE of the ground state of LuO should be in the range of 6.5-7.8 eV,²⁻⁵ which is much higher than the observed 0-0 band energy of 5.5420 (6) eV. Furthermore, previously measured vibrational frequencies by anion photoelectron spectroscopy (839 cm^{-1})²¹ and microwave spectroscopy (816 cm^{-1})²² for the electronic ground state of LuO in the gas phase suggest that the vibrational frequency of LuO (750 cm^{-1}) measured in this work is not associated with the ground state of the molecule.

In an attempt to identify the electronic transition responsible for the MATI spectra, we have carried out an extensive search for the excited states of the neutral molecule and cation at the

MCQDPT2 level. Table 1 lists the bond lengths, harmonic frequencies, and electronic energies relative to the ground state including vibrational zero-point corrections of the neutral and ion states. For the neutral molecule, six doublet electronic states were computed with the ground state being $X^2\Sigma^+$, while for the ion, two singlets and two triplets were computed with the ground state of the cation being $X^1\Sigma^+$. The dominant configurations of the low-lying doublet states of LuO correspond to $\text{Lu}^{2+}\text{O}^{2-}$ with the oxygen 2s and three 2p orbitals doubly occupied and the unpaired electron residing in one of the remaining valence orbitals on lutetium. Figure 2 shows the symmetry unique valence virtual orbitals (VVOs) that give rise to six doublet states of neutral LuO when occupied by the unpaired electron. The $X^2\Sigma^+$ ground state corresponds to the occupation of the Lu 6s orbital while the $C^2\Sigma^+$ and $D^2\Sigma^+$ states correspond to the unpaired electron occupying 6p/5d hybrid orbitals having σ symmetry. The $A^2\Pi$ state has the unpaired electron distributed between the 6p π orbitals that are polarized away from the oxygen, while the $E^2\Pi$ state has the unpaired electron distributed between the 5d π orbitals that are polarized toward oxygen. The remaining doublet state is the $B^2\Delta$ state that has the unpaired electron distributed between the two 5d δ orbitals. The $X^1\Sigma^+$ ground state of LuO^+ corresponds to $\text{Lu}^{3+}\text{O}^{2-}$ with the unpaired electron having been removed from the neutral $X^2\Sigma^+$ ground state. The $A^1\Pi$ and $a^3\Pi$ states of LuO^+ correspond to Lu^{2+}O^+ and can be generated by removing an α ($A^1\Pi$) or a β ($a^3\Pi$) electron from the O 2p π orbitals from the neutral $^2\Sigma^+$ state. Likewise, the $b^3\Sigma^+$ state of LuO^+ has an electron occupying a σ orbital on Lu with an electron removed from the O 2s/2p orbitals. To assess the computational quality, Table 1 also includes the available experimental bond lengths, vibrational frequencies, and electronic energies of several neutral states from previous measurements. To our knowledge, no spectroscopic measurements have been reported for the singly charged cation. As shown in the table, the computed spectroscopic constants agree reasonably with the experimental values, though the energy of the

$C^2\Sigma^+$ state is slightly higher. The good agreement between the calculations and previous measurements give us considerable confidence in the use of the MCQDPT2 calculations to help interpret the MATI spectra.

Table 2 lists allowed ionization processes and energies calculated with MCQDPT2. Among the predicted neutral and ion states, all ionization transitions are allowed, except for $X^1\Sigma^+ \leftarrow B^2\Delta$ and $b^3\Sigma^+ \leftarrow b^2\Delta$, which are forbidden by the $\Delta\Lambda = 0, \pm 1$ selection rule. Among the allowed transitions, only the energies of $a^3\Pi \leftarrow C^2\Sigma^+$ (47430 cm^{-1}) and $A^1\Pi \leftarrow C^2\Sigma^+$ (47916 cm^{-1}) are close to the energy of the 0-0 band (44699 cm^{-1}) of the MATI spectra. Because the intensity profile of $a^3\Pi \leftarrow C^2\Sigma^+$ matches with the experimental spectral profile, the MATI spectrum is assigned to the triplet \leftarrow doublet transition. Although the intensity profile of the LaO and CeO MATI spectra that involve transitions between the ground states of the neutral and ionic molecules is not governed by the FC principle,⁶ the FC intensity of the LuO $a^3\Pi \leftarrow C^2\Sigma^+$ transition appears to be largely consistent with the measured intensity of the cold bands as shown in Figure 1(C) (bottom, black). In Figure 1(C), the calculated T_{00} energy is aligned with the energy of the experimental 0-0 band, but harmonic frequencies are not scaled. The predicted harmonic frequencies are 770 and 654 cm^{-1} for the $C^2\Sigma^+$ neutral state and the $a^3\Pi$ ion state, while the measured fundamentals for these states are 750 and 766 cm^{-1} , respectively. We have tried numerous simulations in a temperature range of $100 - 1500\text{ K}$ and found that the best temperature for producing the $v = 1$ hot band intensity is $\sim 600\text{ K}$. If the simulation temperatures are increased, hot bands at higher vibrational quanta can be produced, but intensities of the hot bands at lower quanta are greatly overestimated. This suggests that the intensities of the hot bands excited from a wide range of vibrational quanta with large vibrational intervals could not be accurately simulated by a single temperature. This is

because vibrational temperatures of molecules seeded in supersonic molecular beams are not at equilibrium and increase with vibrational quanta.

The MATI spectra display the divergence of the vibrational intervals of the ion. While the first three intervals for $v = 1-3$ (766, 767, and 769 cm^{-1}) are within the measurement uncertainty, the fourth interval for $v^+ = 4$ (782 cm^{-1}) is significantly higher. We were not able to extend the measurement to higher vibrational quanta, as our frequency-doubled tunable dye laser could not reach higher photon energies. If the four intervals are fit into a quadratic equation, a harmonic frequency and a negative anharmonicity are obtained as $\omega_e = 761(3)$ and $x_e\omega_e = -2.4(8)$ cm^{-1} . For a diatomic molecule, a negative anharmonicity is practically impossible for a single electronic state as it means that the molecule would not dissociate. A second assignment could attribute the MATI spectra to two transitions: $a^3\Pi \leftarrow C^2\Sigma^+$ with the 0-0 band at 44699 cm^{-1} and $A^1\Pi \leftarrow C^2\Sigma^+$ with the 0-0 band at 46669 cm^{-1} (i.e., the energy of $v^+ = 3$ in Figure 1(A)). This assignment is not consistent with the FC profile of $A^1\Pi \leftarrow C^2\Sigma^+$, which greatly overestimates the intensity of the 782 cm^{-1} band. Thus, we suspect that the two-transition assignment is less likely.

We attribute the observed vibrational divergence of the ion to a vibrational perturbation induced by the interaction between the $a^3\Pi$ and $A^1\Pi$ ion states.^{43,44} As shown in Table 1, the harmonic frequencies of the two states are calculated to be 654 and 660 cm^{-1} , respectively, with the T_{00} energy of the $A^1\Pi$ state 486 cm^{-1} above that of the $a^3\Pi$ state. Based on these calculations, the energies of the $v^+ = 4$ level of the $a^3\Pi$ state and the $v^+ = 1$ level of the $A^1\Pi$ state are 2616 and 2466 cm^{-1} above the T_{00} energy of the $a^3\Pi$ state. The two adjacent vibronic levels are expected to influence each other because the potential energy curves of the two states effectively lie on top of one another. Although selection rules require the interacting states to have the same multiplicity, this restriction is relaxed for lanthanide-containing molecules because of spin-orbit coupling.

Vibrational irregularity is also observed for the neutral molecule, especially at the $v = 8$ (660 cm^{-1}) level (Figure 1A). At lower vibrational quanta, the vibrational intervals are monotonically reduced, suggesting that the neutral vibrational mode is anharmonic with a positive anharmonicity. The abnormality may arise from a perturbation induced by the interaction between the $\text{C}^2\Sigma^+$ state and an electronic state at higher energy by $\sim 5000 \text{ cm}^{-1}$ or more. A recent multireference study reported several states at $\sim 4000\text{-}6000 \text{ cm}^{-1}$ above the $(3)^2\Sigma^+$ state [note: $(3)^2\Sigma^+$ and other states were labeled with a non-standard notation].²⁰ The predominant electron configuration of the $(3)^2\Sigma^+$ state was predicted to have the unpaired electron residing on the Lu atom and having σ symmetry, which corresponds to the dominant configuration of the $\text{C}^2\Sigma^+$ state labelled with the standard notation in our work. Thus, the $(3)^2\Sigma^+$ and $\text{C}^2\Sigma^+$ states are presumably the same state. The higher energy states included what were labeled as $(1)^4\Sigma^+$, $(1)^4\Delta$, $(2)^2\Delta$, $(4)^2\Sigma^+$, $(1)^4\Sigma^-$, and $(1)^2\Sigma^-$. Among these states, the $(4)^2\Sigma^+$ state was predicted at 5155 cm^{-1} above the $\text{C}^2\Sigma^+$ state with a harmonic frequency of 654 cm^{-1} and could interact with $\text{C}^2\Sigma^+$. As the strongly perturbed vibrational level is observed at the $v=6$ level or 5807 cm^{-1} above the vibronic ground state of the $\text{C}^2\Sigma^+$ state, we suspect that the vibrational perturbation occurs between the $v=6$ level of the $\text{C}^2\Sigma^+$ state and the $v=1$ level of the $(4)^2\Sigma^+$ state (i.e., $\text{D}^2\Sigma^+$ in the standard notation in our work), which coincidentally has the calculated energy of 5809 cm^{-1} (i.e., $5155 + 654 \text{ cm}^{-1}$) above the vibronic ground state of $\text{C}^2\Sigma^+$. The perturbation could also affect high vibrational quanta, but the effect should be smaller because the vibrational frequencies of the two states are quite different (745 for the $(3)^2\Sigma^+$ state and 654 cm^{-1} for the $(4)^2\Sigma^+$ state).²⁰ If all observed vibrational intervals are fitted to a quadratic equation, we obtain a harmonic frequency of $\omega_e = 765(5) \text{ cm}^{-1}$ and an anharmonicity of $x_e\omega_e = 4.5(5) \text{ cm}^{-1}$,

which compare well with $\omega_e = 763 \text{ cm}^{-1}$ and $x_e\omega_e = 4.5 \text{ cm}^{-1}$ from rotationally resolved emission spectra.¹⁹

Having explained the abnormality of the vibrational intervals, we now turn to electron configurations of the $C^2\Sigma^+$ neutral state and the $a^3\Pi$ ion state. The predominant configuration of the $C^2\Sigma^+$ neutral is predicted to be $\text{Lu}(5d\sigma^1)\text{O}(2p\sigma^2 2p\pi^4)$ by our MCQDPT2 calculations. If an O $2p\pi$ electron in the $\text{Lu}(5d\sigma^1)\text{O}(2p\sigma^2 2p\pi^4)$ configuration is removed by ionization, the resultant ion states are $^1\Pi$ or $^3\Pi$ depending on the relative orientations of the unpaired $\text{Lu}(5d\sigma)$ and $\text{O}(2p\pi)$ electrons in the $\text{Lu}(5\sigma^1)\text{O}(2p\sigma^2 2p\pi^3)$ configuration of the ion. Because the two unpaired electrons are located on separate atoms, the singlet and triplet Π ions are expected to be close in energy as predicted by our MCQDPT2 calculations. The $a^3\Pi$ state is predicted to be more stable than the $A^1\Pi$ state, which is consistent with Hund's rules.

IV. CONCLUSION

An ionization process involving excited states of LuO ($C^2\Sigma^+$) and LuO^+ ($a^3\Pi$) is identified through threshold ionization spectroscopy and second-order multiconfigurational quasi-degenerate perturbation theory. The ionization spectra show abnormal vibrational intervals in both the neutral and cation states. The abnormality is likely due to vibrational perturbations caused by nearby electronic states. Unlike previously-reported ground-state ionization of LaO and CeO , the intensity of the vibronic transitions associated with the excited states of LuO and LuO^+ is largely governed by the Franck-Condon principle. The computed vibrational frequency of the neutral excited state is in excellent agreement with the experimental value, though the calculations yield a lower fundamental frequency for the excited ion state.

ACKNOWLEDGEMENTS

This material is based upon work supported by the U.S. Department of Energy, Office of Basic Energy Sciences, Division of Chemical Sciences, Geosciences, and Biosciences, Chemical Physics Program, under award number DE-SC0021227 (DSY). GS and MSG were supported by Department of Energy grant AL-20-380-066, administered by the Ames Laboratory, which is operated by Iowa State University under Contract No. DE-AC02-07CH11338.

DATA AVAILABILITY

The data that support the findings of this study are available within the article.

REFERENCES

- ¹ A. Kramida, Ralchenko, Yu., Reader, J. and NIST ASD Team, in *NIST Standard Reference database* (National Institute of Science and Technology (NIST): Gaithersburg, MD 2020, <https://physics.nist.gov/asd> [Mon Jun 28 2021]).
- ² S. G. Lias, in: P. J. Linstrom, and W. G. Mallard, Eds., *NIST Chemistry WebBook, NIST Standard Reference Database Number 69*. (National Institute of Standards and Technology, Gaithersburg, MD, 20899, 2007).
- ³ E. Murad and D. L. Hildenbrand, *J. Chem. Phys.* **73**, 4005 (1980).
- ⁴ J. Kordis and K. A. Gingerich, *J. Chem. Phys.* **66**, 483 (1977).
- ⁵ R. J. Ackermann, E. G. Rauh, and R. J. Thorn, *J. Chem. Phys.* **65**, 1027 (1976).
- ⁶ W. J. Cao, Y. C. Zhang, L. Wu, and D. S. Yang, *J. Phys. Chem. A* **125**, 1941 (2021).
- ⁷ K. P. Huber and G. Herzberg, *Molecular Spectra and Molecular Structure. IV. Constants of Diatomic Molecules*. (Van Nostrand-Reinhold: New York, 1979).
- ⁸ K. Schofield, *J. Phys. Chem. A* **110**, 6938 (2006).
- ⁹ M. Dulick, E. Murad, and R. F. Barrow, *J. Chem. Phys.* **85**, 385 (1986).
- ¹⁰ P. Carette, *J. Mol. Spectrosc.* **140**, 269 (1990).
- ¹¹ P. Carette and M. Bencheikh, *J. Mol. Spectrosc.* **163**, 309 (1994).
- ¹² W. J. Childs, G. L. Goodman, L. S. Goodman, and L. Young, *J. Mol. Spectrosc.* **119**, 166 (1986).
- ¹³ A. Bernard and J. Verges, *J. Mol. Spectrosc.* **201**, 172 (2000).
- ¹⁴ T. C. Steimle and W. Virgo, *J. Chem. Phys.* **116**, 6012 (2002).
- ¹⁵ A. Bernard, F. Taher, A. Topouzhanian, and G. Wannous, *Astron. Astrophys. Suppl. Ser.* **139**, 163 (1999).

- ¹⁶ A. Marquez, M. J. Capitan, J. A. Odriozola, and J. F. Sanz, *Int. J. Quantum Chem* **52**, 1329 (1994).
- ¹⁷ J. Schamps, M. Bencheikh, J. C. Barthelat, and R. W. Field, *J. Chem. Phys.* **103**, 8004 (1995).
- ¹⁸ H. Moriyama, Y. Watanabe, H. Nakano, S. Yamamoto, and H. Tatewaki, *J. Chem. Phys.* **132**, 124310 (2010).
- ¹⁹ A. Bernard and C. Effantin, *Can. J. Phys.* **64**, 246 (1986).
- ²⁰ J. Assaf, R. Reaidi, and R. Assaf, *Computational and Theoretical Chemistry* **1187** (2020).
- ²¹ Z. L. Liu, H. Xie, Q. J. Li, Z. B. Qin, R. Cong, X. Wu, Z. C. Tang, and H. J. Fan, *J. Chem. Phys.* **140** (2014).
- ²² S. A. Cooke, C. Krumrey, and M. C. L. Gerry, *J. Mol. Spectrosc.* **267**, 108 (2011).
- ²³ S. P. Willson and L. Andrews, *J. Phys. Chem. A* **103**, 6972 (1999).
- ²⁴ Y. Liu, L. Wu, C. H. Zhang, S. A. Krasnokutski, and D. S. Yang, *J. Chem. Phys.* **135**, 034309 (2011).
- ²⁵ D. Proch and T. Trickl, *Rev. Sci. Instrum.* **60**, 713 (1989).
- ²⁶ M. A. Duncan, T. G. Dietz, and R. E. Smalley, *J Chem Phys* **75**, 2118 (1981).
- ²⁷ G. M. J. Barca, C. Bertoni, L. Carrington, D. Datta, N. De Silva, J. E. Deustua, D. G. Fedorov, J. R. Gour, A. O. Gunina, E. Guidez, T. Harville, S. Irle, J. Ivanic, K. Kowalski, S. S. Leang, H. Li, W. Li, J. J. Lutz, I. Magoulas, J. Mato, V. Mironov, H. Nakata, B. Q. Pham, P. Piecuch, D. Poole, S. R. Pruitt, A. P. Rendell, L. B. Roskop, K. Ruedenberg, T. Sattasathuchana, M. W. Schmidt, J. Shen, L. Slipchenko, M. Sosonkina, V. Sundriyal, A. Tiwari, J. L. G. Vallejo,

B. Westheimer, M. Wloch, P. Xu, F. Zahariev, and M. S. Gordon, *J. Chem. Phys.* **152**, 154102 (2020).

²⁸ T. Noro, M. Sekiya, and T. Koga, *Theor. Chem. Acc.* **131**, 1124 (2012).

²⁹ M. Sekiya, T. Noro, T. Koga, and T. Shimazaki, *Theor. Chem. Acc.* **131**, 1247 (2012).

³⁰ J. Seino and H. Nakai, *J. Chem. Phys.* **136**, 244102 (2012).

³¹ M. Barysz and A. J. Sadlej, *J. Chem. Phys.* **116**, 2696 (2002).

³² D. Kedziera and M. Barysz, *J. Chem. Phys.* **121**, 6719 (2004).

³³ W. C. Lu, C. Z. Wang, M. W. Schmidt, L. Bytautas, K. M. Ho, and K. Ruedenberg, *J. Chem. Phys.* **120**, 2629 (2004).

³⁴ G. Schoendorff, A. C. West, M. W. Schmidt, K. Ruedenberg, and M. S. Gordon, *J. Phys. Chem. A* **123**, 5242 (2019).

³⁵ G. Schoendorff, A. C. West, M. W. Schmidt, K. Ruedenberg, A. K. Wilson, and M. S. Gordon, *J. Phys. Chem. A* **121**, 3588 (2017).

³⁶ H. Nakano, *J. Chem. Phys.* **99**, 7983 (1993).

³⁷ <http://brettbode.github.io/wxmacmolplt>.

³⁸ B. M. Bode and M. S. Gordon, *J. Mol. Graphics Modell* **16**, 133 (1998).

³⁹ S. Li, "Threshold photoionization and ZEKE photoelectron spectroscopy of metal complexes" *Ph.D. Thesis*, University of Kentucky, 2004.

⁴⁰ Y. Liu, S. Kumari, M. Roudjane, S. Li, and D.-S. Yang, *J. Chem. Phys.* **136**, 134310 (2012).

⁴¹ J. S. Lee, Y. X. Lei, and D. S. Yang, *J. Phys. Chem. A* **115**, 6509 (2011).

⁴² J. S. Lee, Y. X. Lei, S. Kumari, and D. S. Yang, *J. Chem. Phys.* **131**, 104304 (2009).

⁴³ G. Herzberg, *Molecular Spectra and Molecular Structure. I. Spectra of Diatomic Molecules*. (Krieger, Malabar, Florida, 1989).

⁴⁴ H. Lefebvre-Brion and R. W. Field, *Perturbations in the Spectra of Diatomic Molecules*. (Academic Press, Orlando, 1986).

Table 1. Electronic states, equilibrium bond lengths (R_e , Å), harmonic frequencies (ω_e , cm^{-1}), and relative energies including vibrational zero-point corrections (T_{00} , cm^{-1}) of LuO and LuO⁺ from MCQDPT2 calculations.

	R_e	ω_e	T_{00}
LuO			
	1.779	844	
X ² Σ ⁺	(1.7902, ^a 1.7903, ^b 1.7904 ^c)	(844.5, ^a 816, ^b 842.5, ^c 839(10), ^d 829.3 ^e)	0
A ² Π	1.805 (1.805 ^c)	770 (793, ^c 800 ^c)	19729 (19370, ^c 21445 ^c)
B ² Δ	1.800	876	22673
C ² Σ ⁺	1.834 (1.8283 ^c)	770 (763, ^a 770 ^c)	27626 (24402.9 ^{a,c})
D ² Σ ⁺	1.743	848	48084
E ² Π	1.875	796	48506
LuO ⁺			
X ¹ Σ ⁺	1.736	968	55680
a ³ Π	1.945	654	75055
A ¹ Π	1.945	660	75542
b ³ Σ ⁺	1.844	762	80397

^aref 17-electronic emission, 1986

^bref 20-microwave, 2011

^cref 30-electronic emission, 1975. $T_{00} = 19370 \text{ cm}^{-1}$ for $A^2\Pi_{1/2} \rightarrow X^2\Sigma^+$ and $T_{00} = 21445 \text{ cm}^{-1}$ for $A^2\Pi_{3/2} \rightarrow X^2\Sigma^+$.

^dref 19-anion electron velocity-map imaging, 2014

^eref 21-Ar matrix isolation IR, 1999

Table 2. Ionization processes and energies (cm^{-1}) predicted by MCQDPT2 calculations and probed by MATI spectroscopy.

MCQDPT2	$X^1\Sigma^+$	$a^3\Pi$	$A^1\Pi$	$b^3\Sigma^+$
$X^2\Sigma^+$	55680	75055	75542	80397
$A^2\Pi$	35952	55327	55813	60668
$B^2\Delta$	NA ^a	52382	52960	NA ^a
$C^2\Sigma^+$	28054	47430	47916	52771
$D^2\Sigma^+$	7597	26972	27458	32313
$E^2\Pi$	7175	26550	27036	31891
MATI		$a^3\Pi$	$A^1\Pi$	
$C^2\Sigma^+$		44699		

^a $X^1\Sigma^+ \leftarrow B^2\Delta$ and $b^3\Sigma^+ \leftarrow b^2\Delta$ transitions are forbidden as dictated by the $\Delta\Lambda = 0 \pm 1$ selection rule.

Figure captions:

Figure 1. MATI spectra of LuO seeded in a He carrier (a) and an Ar carrier (b) and Franck-Condon simulation at 600 K (c).

Figure 2. Symmetry unique valence virtual orbitals of the neutral LuO molecule. Each of the six doublet states are obtained by singly occupying each of the VVOs.

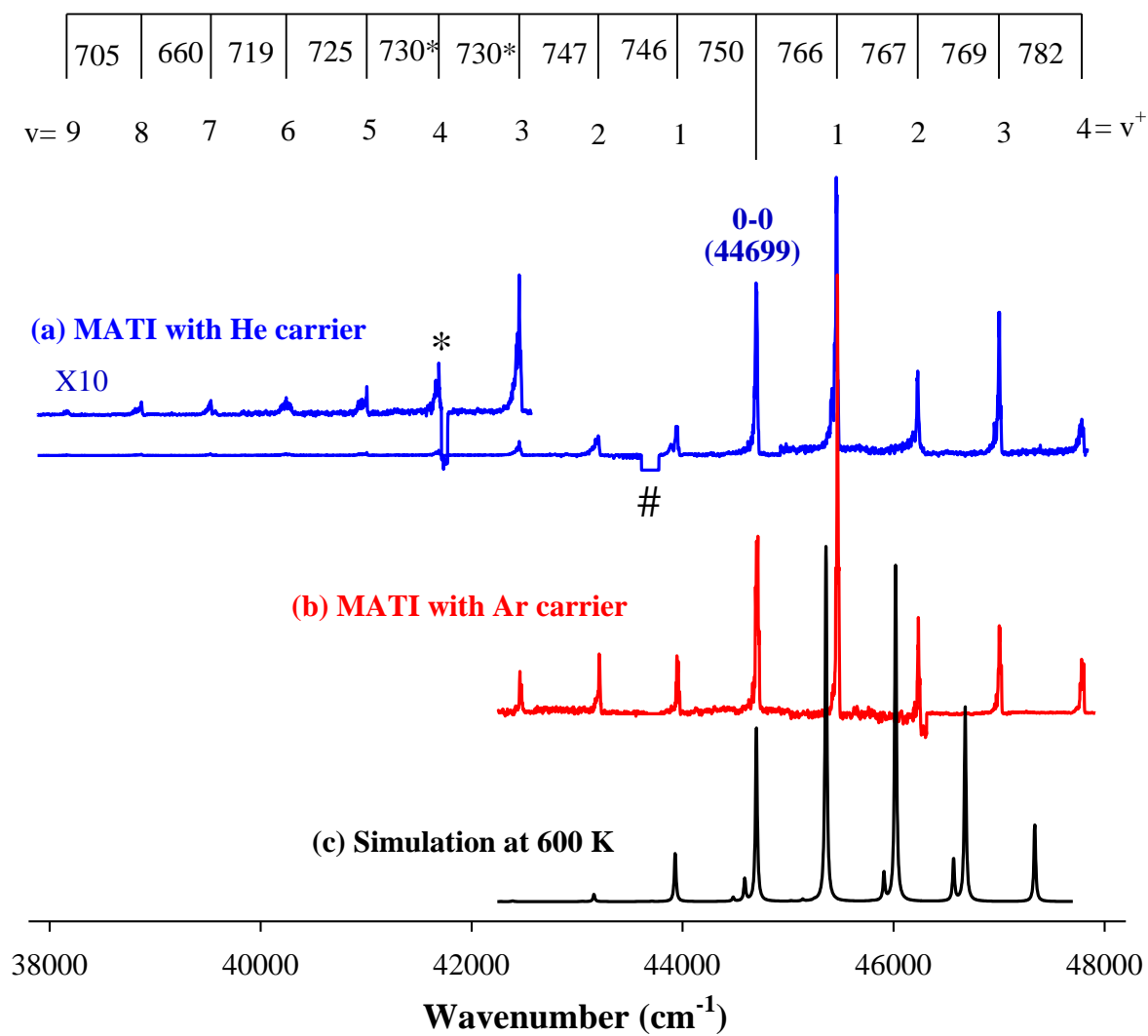


Figure 1

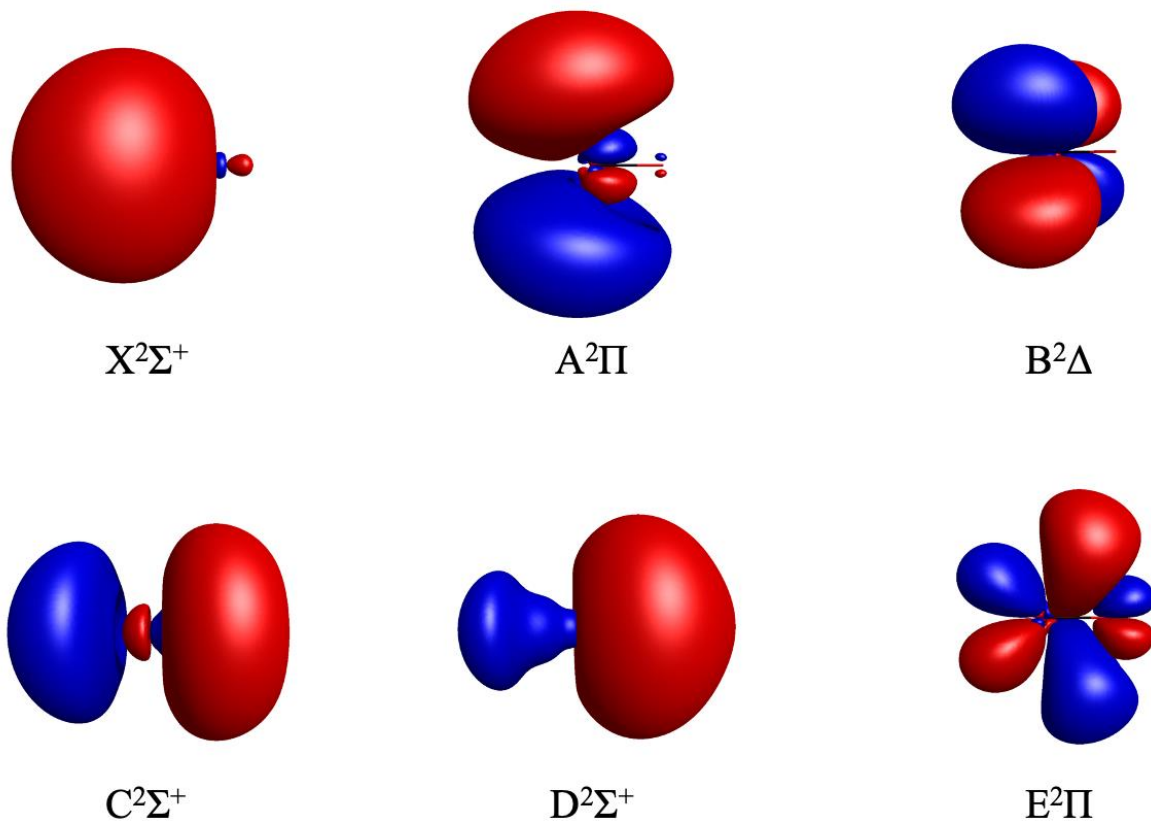


Figure 2

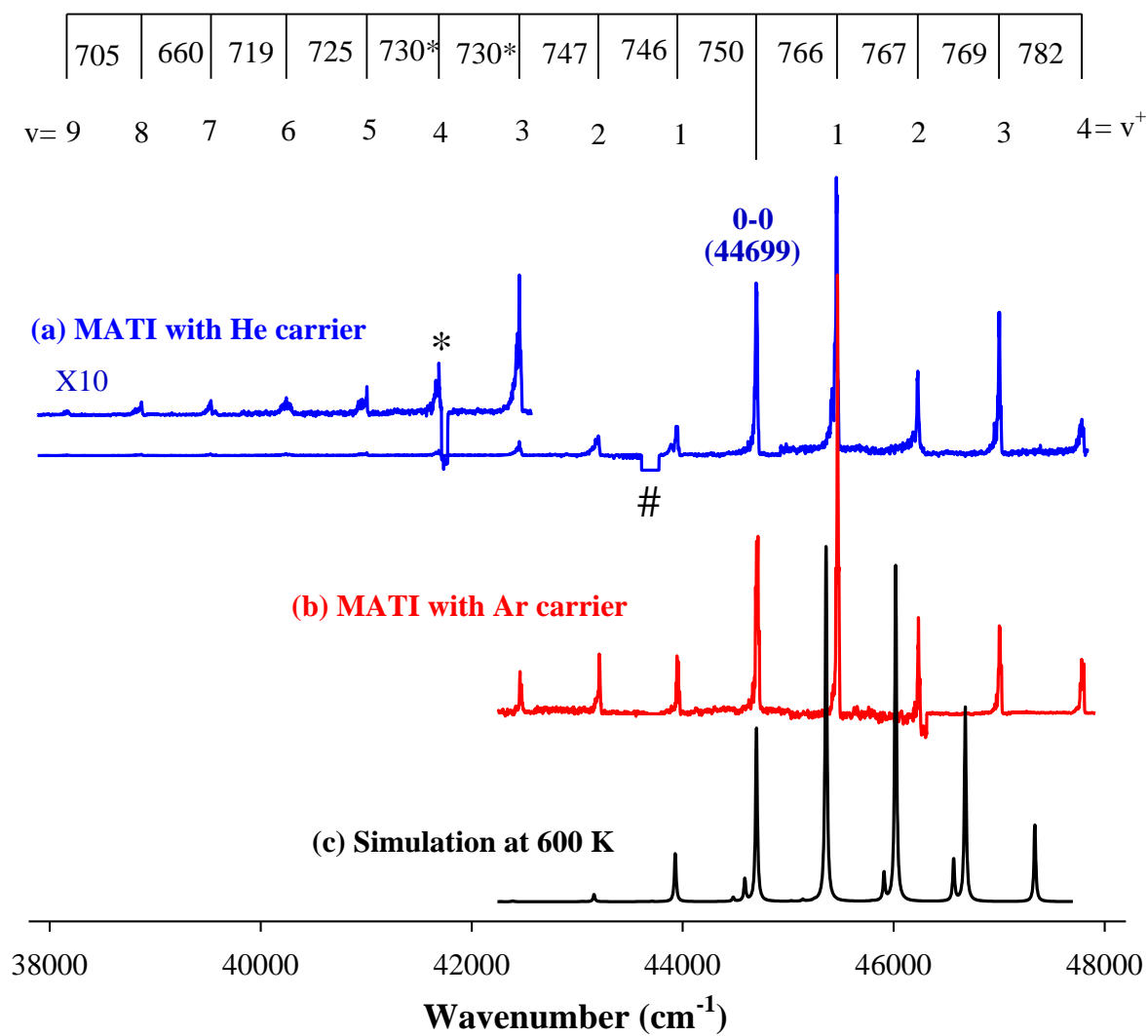


Figure 1

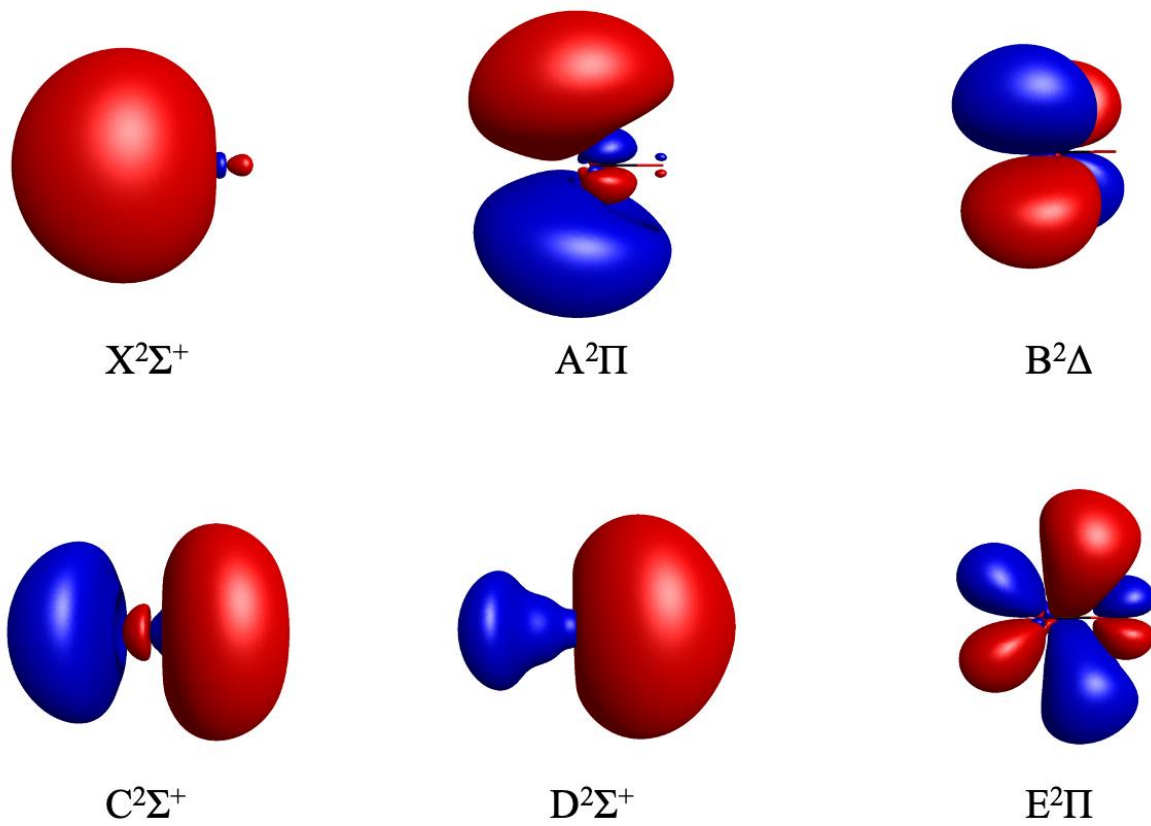


Figure 2